applied sciences

MDPI

Review

Recent Advances in Black Silicon Surface Modification for Enhanced Light Trapping in Photodetectors

Abdulrahman Alsolami [1], Hadba Hussain [1], Radwan Noor [2], Nourah AlAdi [1], Nada Almalki [1], Abdulaziz Kurdi [3], Thamer Tabbakh [1], Adnan Zaman [1,*], Salman Alfihed [1,*] and Jing Wang [4]

[1] Microelectronics and Semiconductor Institute, King Abdulaziz City for Science and Technology (KACST), Riyadh 11442, Saudi Arabia
[2] Future Communication Technology Institute, King Abdulaziz City for Science and Technology (KACST), Riyadh 12354, Saudi Arabia
[3] Advanced Materials Institute, King Abdulaziz City for Science and Technology (KACST), Riyadh 11442, Saudi Arabia
[4] Department of Electrical Engineering, College of Engineering, University of South Florida, Tampa, FL 33620, USA; jingw@usf.edu
* Correspondence: azaman@kacst.edu.sa (A.Z.); salfihed@kacst.edu.sa (S.A.)

Abstract: The intricate nanostructured surface of black silicon (BSi) has advanced photodetector technology by enhancing light absorption. Herein, we delve into the latest advancements in BSi surface modification techniques, specifically focusing on their profound impact on light trapping and resultant photodetector performance improvement. Established methods such as metal-assisted chemical etching, electrochemical etching, reactive ion etching, plasma etching, and laser ablation are comprehensively analyzed, delving into their mechanisms and highlighting their respective advantages and limitations. We also explore the impact of BSi on the emerging applications in silicon (Si)-based photodetectors, showcasing their potential for pushing the boundaries of light-trapping efficiency. Throughout this review, we critically evaluate the trade-offs between fabrication complexity and performance enhancement, providing valuable insights for future development in this rapidly evolving field. This knowledge on the BSi surface modification and its applications in photodetectors can play a crucial role in future implementations to substantially boost light trapping and the performance of Si-based optical detection devices consequently.

Keywords: black silicon; surface modification; light trapping; photodetectors; nanostructures; etching; laser ablation

Citation: Alsolami, A.; Hussain, H.; Noor, R.; AlAdi, N.; Almalki, N.; Kurdi, A.; Tabbakh, T.; Zaman, A.; Alfihed, S.; Wang, J. Recent Advances in Black Silicon Surface Modification for Enhanced Light Trapping in Photodetectors. *Appl. Sci.* **2024**, *14*, 9841. https://doi.org/10.3390/app14219841

Academic Editors: Giovanni Magno, Marco Grande and Ilaria Marasco

Received: 29 August 2024
Revised: 17 October 2024
Accepted: 24 October 2024
Published: 28 October 2024

1. Introduction

Black silicon (BSi) is a material with a high aspect ratio of nano/microscale patterns and order/disorder structures [1–3]. These nano/microscale patterns can be composed of needles or pillar shapes with different sizes [4,5]. The sizes and shapes of surface structures (morphology) of BSi result in remarkable and unique optical properties [6]; thus, the BSi is utilized in various optical applications [7–9]. The BSi was first discovered and published in 1995 by utilizing reactive ion etching (RIE) [10]. Subsequently, in 1998, silicon (Si) surfaces with arrays of sharp conical spikes were created by exposing them to femtosecond laser pulses [11]. Recently, the research frontier of BSi has been expanding at breakneck speed, reaching over 4000 publications over the past five years. Its adjustable properties and capacity for enhancement may improve efficiency in a variety of applications.

One of the noteworthy applications of BSi resides in its capacity to modulate light through the mechanisms of light-trapping phenomena. This innovative approach involves folding light beams multiple times within the absorbing region of optical devices. Thus, BSi significantly reduces transmission losses, allowing for more efficient means for light to be absorbed by the photodetector [12,13]. This process can happen by changing the surface

morphology and roughness [13]. Coating the surfaces with thin films or chemical and physical etching are techniques to change the morphology of the surface and roughness of the material; at the same time, these two ways can also be used to have an antireflection coating or an antireflection structure [14]. With this in mind, the antireflection structures have also shown resistance to destruction from high-energy lasers of nearly 60 J/cm^2 [15]. However, unique properties of the material can be obtained by exercising control over the parameters of the etching methods [16]. The etching methods can be classified into two divisions: wet etching (chemical methods) and dry etching (combined physical and chemical methods). Wet and dry etching as well as laser ablation methods are widely adopted for processing nanoscale features on Si samples, which can dramatically elevate light trapping for Si-based photodetectors, paving the way for improved efficiency [17,18].

The nanoscale features on BSi, including porous structures and needle-like protrusions, effectively enhance the optical properties by trapping the incident light through light scattering and multiple internal reflections, thus minimizing surface reflectance and approaching near-perfect absorption across a broad spectral range [19–21]. Through the etching process and by leveraging the exceptional light trapping capabilities of BSi, a surface engineered by Pengfei et al. through RIE achieved record-low reflectance (~1.1%) across a broad spectral range exceeding 2500 nm. This optimized BSi structure holds significant promise for photothermal applications, including imaging, desalination, and beyond [22]. By laser ablation, particularly with nanosecond pulsed laser ablation, Guanyu et al. successfully tailored Se-doped BSi with remarkable broadband light absorption in the range spanning 400–2200 nm, exceeding 96.81% before annealing and 81.28% after 600 °C annealing. This near infrared (NIR)-enhanced BSi, subsequently integrated into double four-quadrant photodetectors, exhibited exceptional performance metrics with elevation in the responsiveness, a decrease in the dark current, quick response times, and the slightest crosstalk, paving the way for its application in demanding fields like night vision detection and medical imaging [23].

In this work, we present an in-depth review of the recent efforts on the BSi chemical and physical processing, with a keen interest in leveraging the BSi structures for light trapping to improve the performance of photodetectors. The foundational work of others, as well as our own work, is discussed to explore the essential micro- and nanofabrication process considerations of BSi. The meticulous analysis of processing impact on BSi is instrumental to lay the groundwork for future developments in surface modification techniques for microstructures in Si-based optical devices.

2. Wet Methods for Black Silicon Fabrication

This section explores the techniques used for wet chemical etching to modify the surface of BSi. Wet etching offers a cost-effective and versatile approach to achieving nanostructured surfaces. The most common wet-etch-based methods for BSi are discussed herein, including metal-assisted chemical etching (MACE), potassium hydroxide (KOH) etching, and electrochemical etching.

2.1. Metal-Assisted Chemical Etching (MACE)

The MACE is a highly inexpensive and efficient technique, utilizing various metal elements such as silver (Ag), copper (Cu), nickel (Ni), and aluminum (Al). The process involves submerging a meticulously cleaned and deoxidized sample in an etching solution, leading to the creation of metal nanoparticles (NPs) on the Si surface. This drives an improvement in the light-trapping performance and influences the sample's reflectivity. It is worth noting that each element has its distinct characteristics that impact the resulted BSi surface and structure. For instance, Ag ions affect the porosity of BSi, Cu offers better optical absorption properties, Ni can fabricate BSi surface in less process steps, while Al enables precise control over the morphology of the nanopores. The following paragraphs will discuss assisted chemical etching based upon Ag, Cu, Ni, and Al, with keen interest in their corresponding etching impact on the BSi surface and resultant optical response.

2.1.1. Silver-Assisted Chemical Etching

As this process can be used to create intricate nanostructures on Si surfaces, Li et al. utilized Ag-assisted chemical etching to enhance the light-trapping efficiency and the performance of multi-crystalline BSi solar cells [24]. This has been achieved by introducing an additive to create uniform nanostructures on crystalline samples, as shown in Figure 1. The nanostructures exhibited uniform depth and diameter, along with exceptional properties. The Ag-assisted chemical etching method, along with the additive, is a highly effective approach for large-scale, high-efficiency, multi-crystalline BSi solar cell production. It is worth noting that the average efficiency of the solar cells was raised from 0.64% to 19.24% using the MACE process.

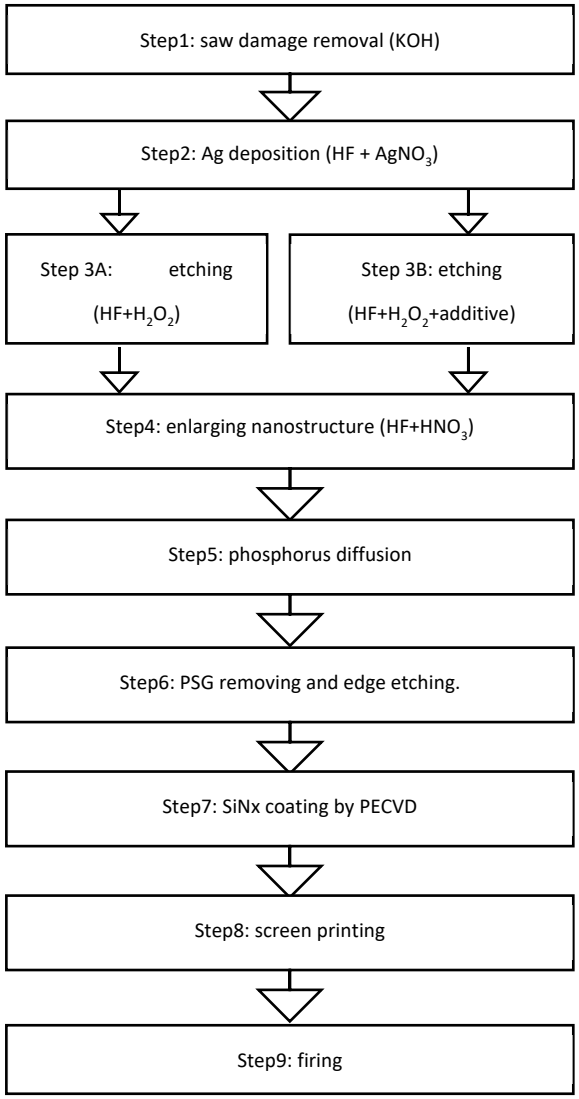

Figure 1. Schematic process-flow diagram of the experimental method to enhance light-trapping efficiency through Ag-assisted chemical etching. The diagram illustrates the application of an additive for creating uniform nanostructures, which significantly increased cell efficiency. The schematic details the uniformity of nanostructure depth and diameter, highlighting the method's effectiveness for large-scale high-efficiency solar cell production [24].

Furthermore, Noor et al. explored the relationship between the etching time and the absorption enhancement of broadband light in BSi [25]. Ag was thinly applied to Si samples and then heated in a nitrogen (N_2) environment to create Ag NPs. Subsequently, the etching process was in a mixture solution of hydrofluoric acid (HF), hydrogen peroxide

(H_2O_2), and liquid water (H_2O) (HF:H_2O_2: H_2O) for unlike intervals at room temperature, leading to the formation of BSi. The BSi nanotextures created a rough surface morphology, which reduced broadband optical reflection. It has been observed that the crystalline Si (c-Si) samples etched for 70 s exhibited the lowest broadband reflection, reaching 3% at a wavelength of 600 nm. The BSi nanotextures in this sample were between 50 and 100 nm in width and 300 and 400 nm in height.

Abdulkadir et al. have successfully optimized the etching time for enhancing broadband absorption in BSi, with an ultimate goal of increasing the efficiency of solar cells [26]. Their method involved using the one-step electroless Ag-assisted chemical etching method, which produced BSi nanowires with a diameter of approximately 100 nm and heights ranging from 2.0 to 2.9 µm. Notably, after etching for 80 s, BSi nanowires with a height of 2.9 µm exhibited 94% absorption at 600 nm. On a related note, Venkatesan et al. investigated the effects of Ag catalyst concentration in MACE on the mechanisms of nanostructure formation on Si and their optical properties [27]. They employed HF along with silver nitrate ($AgNO_3$) concentrations of 2 mM, 3 mM, 4 mM, and 8 mM to create p-type Si nanostructures. The experimental results showed that the decrement of catalysis molarity concentration during etching processes led to the creation of nanostructures ranging from 140 to 60 nm, thereby offering valuable insights into their formation. These nanostructures were found to form BSi, causing a reduction in reflectance and demonstrating that MACE holds great promise as a method for antireflection coatings on BSi-based solar photovoltaic (PV) cells. Both studies exemplify significant advancements in nanofabrication techniques aimed at reducing reflectance and enhancing light trapping.

In addition, an examination was conducted of the Ag thin films' thickness influence on the morphological and optical characteristics of BSi, created via two-step Ag-assisted chemical etching. They found that a 15 nm thin film of Ag led to surface coverage of Ag NPs at approximately 72.5%, forming dense, spherical shapes with an average nanopore height and diameter of about 420 nm and 200 nm, respectively [28]. This configuration led to an improvement in optical absorption across the wavelength spectrum of 300 to 1100 nm. Concurrently, Tang et al. conducted a study on Si substrates to generate inverted pyramids of varying sizes from the micron to sub-micron scale via MACE with temperature control [29]. Utilizing a mask-free silver-assisted chemical etching process, succeeded by a subsequent step to reconstruct nanostructures, they effectively demonstrated this method as a viable light-trapping mechanism. Both studies use innovative approaches to structuring Si for improved light absorption in solar cell applications, with significant implications for enhancing PV efficiency [30].

2.1.2. Copper-Assisted Chemical Etching

In their respective studies, Park et al. and Zhao et al. explored the impacts of MACE on the optical characteristics of BSi [31,32]. It was found that Cu-assisted chemical etching achieved a reflectivity of 5.92% after 90 min, although this result varied across the sample as etching time increased. Notably, a lower reflectivity of 3.96% was observed after 5 min of etching, attributed to the formation of more homogenous pores that minimized reflectance. Similarly, Zhao et al. employed Cu-assisted chemical etching to engineer various surface textures on monocrystalline Si solar cells [32]. Their method effectively produced an array of structures including inverted pyramids, nanopores, upright pyramids, V-grooves, and hybrid structures. This innovative one-step technique not only facilitated the creation of random inverted-pyramid structures on Si samples but also enhanced light-trapping capabilities, significantly reducing reflectance and lowering production costs. Together, these studies underscore the Cu-assisted chemical etching potential to optimize the surface properties, thus improving the light trapping of Si-based solar cells.

2.1.3. Nickel-Assisted Chemical Etching

The Ni-assisted chemical etching process was utilized by Volovlikova et al. to investigate the impact of different etching regimes on BSi reflection [33]. The BSi with a

thickness of 580 nm, which was produced under illumination for 60 min, demonstrated exceptionally low reflectance measurements of 2.3% within the ultraviolet (UV) spectrum (200–400 nm), 0.5% in the visible spectrum (400–750 nm), and 0.3% in the infrared spectrum (750–1300 nm). These findings highlight the significance of the thickness and duration of treatment in determining BSi reflectivity, which has a direct impact on the detection response of the optical devices. In addition, Ni NPs can be eliminated during the etching procedure, thus saving time by reducing the cleaning steps required to eliminate them [34].

2.1.4. Aluminum-Assisted Chemical Etching

Al-assisted chemical etching was investigated in several studies by Uddin et al. for the optimization of BSi surface properties [35]. In their first study, they manipulated the surface morphology of nanoporous BSi by varying the thickness of the Al catalyst and the concentrations of HF and H_2O_2 in deionized water. The study revealed that a catalyst thickness of 24 nm, combined with a specific composition of HF-H_2O_2-H_2O, had a considerable impact on the morphology of the nanopores, resulting in a minimum broadband average reflection (R_{avg}) of 5.7%. This finding is critical for optimizing the performance of PV cells and photosensors. In a subsequent study, Uddin et al. further explored the Al-assisted chemical etching technique, observing how the thickness of the Al layer affected nanopore formation [36]. With a 12 nm thickness, a decrease in pore depth and lower surface coverage is noted, leading to a higher R_{avg} of 11.9% within the 300–1100 nm wavelength range. However, this setup also produced the highest broadband light absorption, indicating a trade-off between pore coverage and absorption efficiency. Ultimately, they investigated the impact of annealing temperature on BSi properties [37]. Annealing at 400 °C led to the deepest and most extensively covered nanopores, producing the minimal broadband reflection in the 300–1100 nm range. This treatment achieved an average enhancement in absorption of 1.61, significantly surpassing that of a planar c-Si reference, thereby illustrating the potential of thermal treatment to further enhance the light absorption properties of BSi. The aforementioned studies illustrate the effects of process variables on BSi's structural and optical characteristics, which significantly contribute to the development of efficient optical detection mechanisms.

2.2. Potassium Hydroxide (KOH) Etching

The wet chemical etching technique of Si entails submerging the Si sample in chemical(s), commonly KOH, to generate a micro-pyramidal texture on the surface of Si sample. This procedure selectively eliminates unwanted material layers while preserving the protective layer's integrity. The speed of etching is contingent on three essential factors: the solution's temperature, the length of time involved in the etching procedure, and the etchant's concentration. The study conducted by Ibrahim et al. delved into the changes that occurred in the structure and appearance of boron-doped porous Si (B-P-Si) following an etching process using KOH [38]. Field Emission Scanning Electron Microscopy (FESEM) was employed for the characterization of surface properties. Notably, the FESEM images displayed the formation of etching patterns and pores, with optical reflectance values of 2.8% and refractive indices of 1.8. Additionally, the Hall effect measurements demonstrated a significant increase in electrical conductivity.

In an effort to enhance the efficiency of light trapping, an experiment of KOH etching was utilized to study its influence on BSi surface [39]. The ultimate aim was to fine-tune the parameters that enhance PV efficiency and a numerical simulation was utilized to analyze the results. The study demonstrated that anisotropic etching created a textured surface on BSi samples, which reduced their reflectance and resulted in a 2% increase in efficiency. Additionally, the researchers optimized the doping concentrations for the p-type and n-type, resulting in a remarkable 23.14% conversion efficiency for PV made from BSi samples. This study represents a significant leap forward in improving the effectiveness of PV technology through enhancing the surface properties.

2.3. Electrochemical Etching

The electrochemical etching method involves using Si as the anode, which is then submerged in a solution of HF, H_2O, and ethanol. A cathode made of platinum is also employed for its conductivity and resistance to HF. The aim of this method is to reduce reflectivity by precisely controlling both the etching time and current density. Zhong et al. created a porous Si photonic crystal architecture on a c-Si via electrochemical etching conducted at ambient temperature [40]. This was conducted to enhance surface properties for Raman scattering sensors and optical detection devices. The surface roughness affected porosity and pore size distribution but not the vertical etching rate. The obtained results indicate significant light scattering effects and lattice compression. A reflectance of approximately 1% across a wide range of wavelengths (400–700 nm) was recorded, highlighting the significant potential of rear-side porous Si photonic crystals for use in photonics applications.

Furthermore, low-reflective samples have been prepared on a p-type <100> Si substrate using various electrochemical etching currents/durations, which are suitable for optoelectronic applications [41]. The BSi was analyzed by FESEM, revealing layer formation with porosity percentages ranging from 10 to 40%. The reflectivity assessment demonstrated a reduction in intensity and a shift towards longer wavelengths with increasing etching current, ultimately resulting in peak photoluminescence at 360 nm.

Overall, wet chemical etching techniques are utilized for BSi surface modification. Cost-effective and versatile methods like MACE, KOH etching, and electrochemical etching, which are commonly used to create nanostructured BSi surfaces, are discussed. The MACE technique uses metal elements (Ag, Cu, Ni, and Al) to produce metal nanoparticles on silicon surfaces. Thus, it enhances light trapping and reflectivity. Each metal influences the surface differently, where Ag affects porosity, and the etching rate in their proximity is significantly elevated. Cu improves light absorption and inverted pyramid formation; Ni NPs disappear during the etching process, the Ni NPs cleaning step is eliminated, and, thus, the etching process steps are decreased. Al NPs have high control over the nanopores' morphology. The KOH etching technique exhibits high controllability by manipulating concentration, temperature, and etching duration. This method facilitates the straightforward fabrication of BSi surfaces. The anisotropic etching process forms a textured surface on the BSi samples, significantly reducing reflectance. Electrochemical etching created a porous Si through ambient temperature for porosity and pore size distribution but not vertical etching rate to reduce reflectivity by precisely controlling the current density and etching time and recording an extremely high light trapping with a reflectance of approximately 1% across the visible range and controlling the porosity percentages of layer formation. A comprehensive review of the recent developments in BSi using wet etching methods is shown in Table 1.

Recent advancements in photodetector fabrication techniques have demonstrated significant performance improvements, particularly through surface modification strategies. Black silicon, known for its superior light-trapping capabilities, has been widely used to enhance photodetector efficiency, especially in the infrared region. Wet etching techniques, particularly metal-assisted chemical etching (MACE), have been central to creating nanostructured black silicon surfaces that improve light absorption. In parallel, water-assisted transfer printing has emerged as a novel method for fabricating organic photodetectors, offering fast rise times and a high on/off ratio due to the use of a sacrificial ethylene glycol-doped PEDOT layer. This method has proven effective in overcoming surface adhesion challenges, thus potentially opening pathways for integrating organic layers with black silicon surfaces. The synergy between these techniques could lead to hybrid photodetectors with enhanced responsivity and light-trapping capabilities across a broader spectrum [42]. Material modifications play a crucial role in optimizing the performance of advanced photodetectors. Just as the addition of plasticizers, like glycerol, has been shown to influence the molecular mobility and morphology of poly(vinyl alcohol) (PVA) films, surface modifications in black silicon significantly affect its light-trapping capabilities

and overall efficiency in photodetectors. Recent studies on PVA films demonstrate how plasticization can decrease crystallinity while increasing the mobility of the polymer chains, therefore, leading to enhanced mechanical properties and flexibility. Similarly, surface treatments of black silicon aim to fine-tune the material's structural and optical properties, improving its performance in light detection applications [43].

Table 1. A summary of the recent work in surface modification of BSi by using wet chemical etching for light-trapping applications in optical devices.

Objectives	Method	Findings	Ref.
Enhance efficiency of multi-crystalline BSi	MACE (Ag)	Significantly increased efficiency and optical performance in multi-crystalline BSi solar cells, demonstrating the effectiveness of MACE in enhancing PV cell capabilities.	[24]
Investigate etching time effects BSi absorption	MACE (Ag)	Identifying optimal etching durations resulted in a significant reduction in broadband reflectance and a considerable enhancement in absorption efficiency, underscoring the essential influence of etching time on optimizing the optical performance of BSi.	[25]
Optimize etching time and study Ag concentration effects	MACE (Ag)	Enhanced broadband light absorption achieved through careful optimization of etching times and silver concentrations, resulting in significant improvements in BSi optical efficiency.	[26,27]
Develop various BSi texturizations and study MACE parameters' effects.	MACE (Ag)	Development of varied texturizations, including nano-pyramidal and nano-grass structures, improved antireflective properties and overall efficiency of BSi. Adjustments in MACE parameters led to optimized optical properties.	[44–49]
Investigate Ag film thickness effect	MACE (Ag)	Varying the Ag film thickness critically affects BSi optical and morphological properties. Temperature control during etching influenced the formation of large, inverted pyramids, optimizing light trapping on Si surface.	[28,29]
Achieve high efficiency in Si solar cells with BSi.	MACE (Ag)	Creation of hierarchical BSi textures resulted in ultra-low reflectance and omnidirectional light-trapping capabilities, leading to improvements in the c-Si optical properties.	[50]
Study Cu-assisted chemical etching and regulate surface texturization	MACE (Cu)	Cu-assisted chemical etching yielded uniform low-reflectance BSi and diverse texturized surfaces, significantly improving the antireflective performance and overall efficiency of Si solar cells.	[31,32]
Study Ni-assisted chemical etching impact on reflection.	MACE (Ni)	The use of Ni-assisted chemical etching effectively minimized reflectance across UV, visible, and infrared spectrums, demonstrating its effectiveness in creating highly efficient light absorbing BSi films.	[33]
Study catalyst thickness and annealing effects	MACE (Al)	Investigations into the impact of Al catalyst thickness and annealing on BSi revealed that these factors critically influence surface morphology and reflectivity, leading to optimal conditions for enhanced light absorption suitable for PV applications.	[35–37]
Investigate morphological properties	KOH	The etching process created BSi surfaces with significantly reduced reflectance and high conductivity, thereby enhancing the overall efficiency and performance of solar cells. Optimization of these processes was crucial for improved solar cell applications.	[38,39]
Study optical properties of Si photonic crystals	Electro-chemical Etching	Porous Si photonic crystals exhibited strong light scattering effects and low reflectance, enhancing their utility in photonic applications.	[40,41]

3. Dry Methods for Black Silicon Fabrication

The BSi microfabrication process employs a toolbox of dry microfabrication techniques to precisely sculpt microscopic features. This typically involves RIE methods for controlled material removal, ion implantation for introducing specific dopants into the material, plasma etching for creating intricate patterns, and even femtosecond laser pulses for ultra-fast and high-precision ablation. A review of the recent works in dry etching for BSi fabrication is presented in the following subsections.

3.1. Reactive Ion Etching (RIE)

The RIE method, commonly employed through fluorine-based processes to create BSi, involves the use of sulfur hexafluoride (SF_6) and oxygen (O_2) as etching gases [51–55]. These gases generate fluoride and O_2 radicals as part of the etching process. Specifically, the fluoride radicals are responsible for etching the Si by eliminating the volatile silicon tetrafluoride (SiF_4) that is produced. Simultaneously, the O_2 radicals become ionized and then interact with both Si and fluoride radicals, resulting in the development of a passivation layer. This passivation layer, also referred to as a polymeric film, serves as a thin protective coating during the etching process. It is partly removed due to continuous energetic ion bombardment. This repeated cycle of passivation and etching ultimately leads to the emergence of randomly distributed nanostructures on the surface that exhibit a needle-like morphology.

One of the most crucial characteristics of BSi that makes it suitable for use in optical and photonic applications is its antireflective property. This feature can be attained through intrinsic lattice modifications or the enhancement of additional substances. Numerous studies have delved into further investigation. For instance, Zhang et al. successfully created BSi with unique chimney-like hierarchical micro/nanostructures using a two-step RIE process [52]. Following that, gold (Au) NPs were deposited onto the BSi using magnetron sputtering deposition, as shown in the scanning electron microscopy (SEM) images in Figure 2. By combining the hierarchical texture with specific-sized Au NPs, they were able to achieve an exceptionally low broadband reflectivity of BSi, measuring less than 1% across a wavelength spectrum extending from 220 to 2600 nm. The nanopores obtained in this work by Zhang et al. exhibit a 6.5 µm and less than 450 nm average depth and diameter, respectively. The attainment of a notably high aspect ratio for these nanopores was achieved through the deliberate adjustment of the SF_6/O_2 gas flow ratio. Specifically, the SF_6/O_2 gas flow ratio for achieving the desired nanostructures was set to 36:47 (increasing the gas flow of O_2 by 30% than that of SF_6). This selection was predicated upon the abundance of O_2 radicals, which expedited the swift development of a silicon oxide (SiO_x) layer on the lateral surfaces throughout the etching procedure. Consequently, this induced a highly selective etching predominantly in the downward direction, ultimately resulting in the formation of nanopores characterized by an extremely high aspect ratio.

Furthermore, François et al. conducted a study in which BSi nanostructures were fabricated at room temperature and characterized by both high aspect ratios and remarkable absorptance using RIE (RT-RIE) [53]. Within the visible and near-infrared (NIR) spectra, the absorption efficiencies exceeded 99%. In this study, four distinct samples were processed with varying etching parameters, resulting in diverse nanostructures within the BSi material. Notably, the sample with the tallest nano-cones that was achieved through specific etching parameters exhibited the highest absorptance across the entire visible spectrum. The key parameters for the optimal BSi etching included an SF_6/O_2 ratio of 1.3:1, a pressure of 5 mTorr, a power of 20 W, an etching duration of 20 min, and a bias of 177 V, which led to the formation of randomly distributed nano-cones of approximately 850 nm in height.

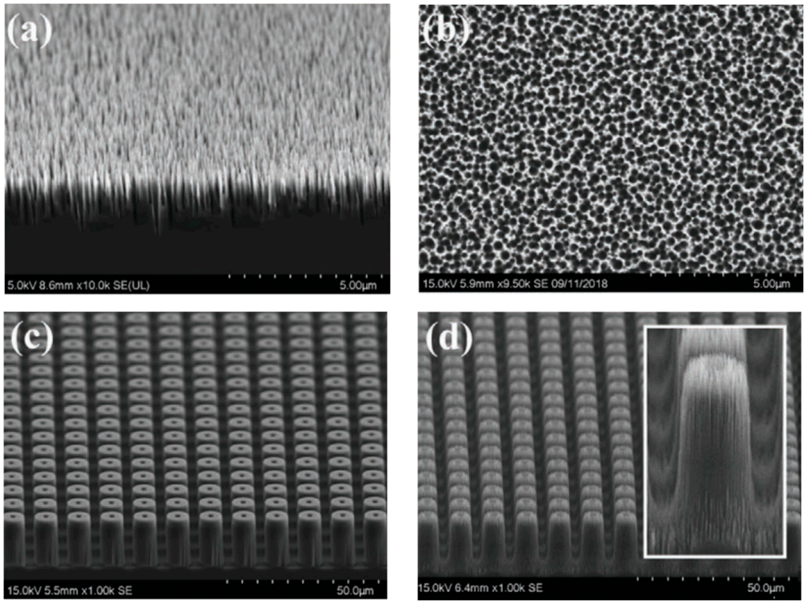

Figure 2. (**a**) The top-view SEM images of BSi with nanopores, (**b**) the side-view SEM images of BSi with nanopores, (**c**) an inclined view of the BSi surface with hollow cylinders, and (**d**) an inclined view of chimney-like BSi with a hierarchical structure [52], © 2020 The Authors. Published by WILEY-VCH Verlag GmbH & Co. KGaA, Weinheim.

The RIE method is also used to fabricate BSi that results in a nano-texture that greatly reduces reflectance across a broad range of wavelengths, approaching zero reflectance [54]. The intricate interplay between the fabrication process and the resultant nanotexture posed significant challenges in improving the electrical characteristics of the phosphorus emitter. The samples were diffused with a phosphorus oxychloride ($POCl_3$) and O_2 ratio of 450/600, respectively, in order to minimize the phosphorous atoms in the Si. This led to decreasing dopant surface concentrations. Through applying corona charges, the emitter recombination factor quality has been improved significantly close to the industrial standards in the order of ~30 fA/cm^2.

Additionally, BSi was fabricated using the RIE method under various parameter conditions to investigate the effects of roughness on the samples [55]. The applied pressure in the process showed a linear relationship with the surface topologies. Furthermore, the RIE technique demonstrated superior surface roughness in comparison to alternative methodologies, including Plasma Immersion Ion Implantation (PIII) and wet etching processes.

3.1.1. Deep Reactive Ion Etching (DRIE)

The Deep Reactive Ion Etching (DRIE) method is a commonly used technique for fabricating BSi or nanostructured Si with a high aspect ratio, enabling efficient light absorption. DRIE involves cyclic time-multiplexed etching, alternating between two cycles as in Equations (1) and (2): a cycle of octafluorocyclobutane (C_4F_8) plasma deposition utilizes fluorocarbon species to deposit a polymer film of difluorocarbene (CF_2) on the Si surfaces, including the sidewalls followed by a plasma etching cycle that employs ions to etch the Si and the deposited film. The desired etching profile is achieved by repeating the cycle process multiple times. In the etching cycle, the SF_6 splits into chemically metastable sulfur tetrafluoride (SF_4) and two individual fluorine (F) atoms.

$$C_4F_8 \rightarrow -(CF_2)_4- \rightarrow Polymer \quad (1)$$

$$SF_6 \rightarrow SF_4 + 2F \rightarrow Etching \quad (2)$$

An improved DRIE method introduced by Maha et al. systematically tuned the polymer deposition time to SF_4 fabricate nanostructured BSi (n-BSi) in micrometer-scale

absorptive regions of high-contrast optical alignment marks [56]. Adjusting the deposition time, while maintaining other parameters as fixed, resulted in three distinguished etching regimes. The unruffled etching regime, characterized by equal or longer etching times compared to deposition, produced a vertical profile with scalloped sidewalls. The n-BSi regime, occurring when etching time closely matched the deposition time, utilized the nano-masking effect to create n-BSi structures. The etch-stop regime occurred when deposition time significantly exceeded etching time, halting the etching process. Increasing the time within the n-BSi regime led to a morphological transformation from nanopillars to nanopores. In our prior work, we noted a substantial enhancement in the growth of grass structures when the substrate temperature dropped below −20 °C. We identified the cyclic Bosch process, involving etching and passivation stages, as a crucial factor in the formation of these structures. Furthermore, we found that the interaction between SF_6 and O_2 gases during the Bosch process played a pivotal role in the formation of microstructures [57]. Figure 3 shows an SEM image of BSi formation (as grassy-looking residuals) by controlling the etch profile due to micro-masking.

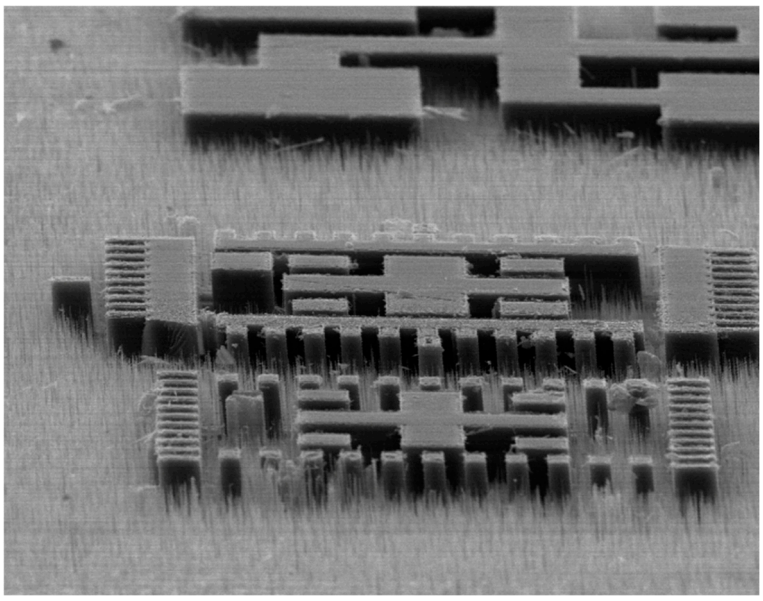

Figure 3. An SEM image of BSi (as grassy-looking residuals) on the etch profile due to micro-masking caused by excess polymer from increased C_4F_8 pulse time and incomplete O_2 plasma etching.

3.1.2. Inductively Coupled Plasma Reactive Ion Etching (ICP-RIE)

The fabrication of BSi can also be achieved through the utilization of the inductively coupled plasma reactive ion etching (ICP-RIE) process. Typically, this process employs SF_6 as the primary etchant gas. The introduction of O_2 into the process serves to promote the formation of silicon oxyfluorides ($SiOF_2$), which serves as an efficient passivation layer. Consequently, this enables an anisotropic etching process, resulting in the formation of randomly distributed needle-like nanostructures [58].

A pioneering study by David et al. ICP-RIE was employed to fabricate BSi on hemispherical Si lenses with a radius of 12.7 mm, enabling the first-ever examination of nanostructures on such highly curved surfaces [58]. By systematically adjusting the etching parameters, including a critical etching pressure of 2 Pa and gas flows of SF_6 and O_2 at 60 sccm, the team successfully replicated diverse structural morphologies akin to those achievable on flat Si samples. The uniformity and orientation of these structures across the lens surface were meticulously analyzed through SEM. Optical reflectance measurements validated the findings, confirming uniformity and demonstrating significantly reduced reflectance, pivotal for the augmentation of optical systems performance in infrared and terahertz technologies. This study not only opens new avenues for applying BSi in nonpla-

nar device architectures but also underscores the adaptability and potential of ICP-RIE for advanced manufacturing processes.

The large-area tomography technique integrates plasma focused ion beam and SEM, which could characterize BSi morphologies over expansive areas up to 320 μm^2 [59]. A quantitative two-dimensional (2D) dopant mapping with an optimized SEM was employed for dopant contrast imaging (SEMDCI), capable of effectively analyzing textured surfaces like BSi. The direct integration of these morphological characterizations with optical properties via FDTD simulations provides a robust framework for enhancing BSi applications in photovoltaics and sensor technologies, which aimed to boost their performance and efficiency.

A temperature of -5 °C and a pressure of 20 mTorr were utilized in our prior work and SF_6/O_2 flow rates of 85/18 sccm. The RF and Induced Coupled Plasma (ICP) powers were set at 100 W and 300 W, respectively. We employed a planar ICP source and a capacitively coupled radiofrequency (RF) source to enable precise control of ion energy independently of plasma density, a crucial factor in producing uniform nanostructures that is essential for high-quality BSi. These specific parameters were strategically selected based on extensive research correlating them with the successful fabrication of BSi with desired morphological and optical properties. Creating BSi via ICP is a sophisticated process that requires a comprehensive understanding of the etching environment to consistently produce it for advanced applications. Its distinctive surface properties make BSi particularly advantageous for PV applications, where it can improve the efficiency of photodetectors [60].

3.2. Ion Implantation Process

Ion implantation represents another frequently utilized technique for generating BSi [61]. This approach utilizes high-voltage pulsed direct current (DC) or pure DC power to accelerate ions toward an appropriate substrate independent of plasma dependence.

Ion implantation has been used to fabricate sulfur (S)-doped Si nanowire arrays, referred to as BSi [62]. This work explored how the morphology of Si nanowires influences absorption across the complete wavelength range of 0.3–2.5 µm and examined the impacts of thermal annealing on below-bandgap absorption. It was revealed that S-doped BSi demonstrates enhanced absorbance across the complete wavelength spectrum of 0.3 to 2.5 µm when contrasted with undoped Si nanowire arrays and flat Si. Meanwhile, a study by Gao et al. successfully employed PIII using SF_6 and O_2 to fabricate polycrystalline BSi [63]. Subsequently, a defect removal etching process was implemented under a range of conditions, with the objective of diminishing surface recombination by decreasing surface area and alleviating damage from plasma etching. The researchers investigated the surface microstructures, reflectance, and internal quantum efficiency of the BSi utilizing an FESEM, a spectrophotometer, and a quantum efficiency measurement apparatus, respectively. Their studies indicated improvements in all these aspects. SEM images revealed that, with increased defect removal etching (DRE) process time, the height and density of nano-hills on the BSi surface decreased, which corresponded to a reduction in surface reflectance.

Ion implantation is a promising and suitable technique for boron doping in next-generation c-Si solar cells, but its application has been traditionally limited by the necessity for high activation annealing temperatures, typically around 1050 °C. In their study, Lanterne et al. utilized PIII with a diborane (B_2H_6) gas precursor, successfully reducing the required annealing temperature to as low as 950 °C [64]. This modification not only preserved a high quality of emitters but also substantially enhanced the efficiency of n-type passivated emitter rear totally diffused solar cells, achieving a performance level of 20.8%. These findings are vital for reducing manufacturing costs and enhancing the viability of ion implantation in large-scale solar cell production.

3.3. Plasma Etching

The developed BSi using a novel plasma etching technique known as Clear, Oxidize, Remove, and Etch (CORE) has diverged from traditional methods by replacing the

fluorocarbon inhibitor in the RIE process with O_2 [65]. This adaptation leverages the self-regulating characteristics of the oxidation phase, thereby improving the synthesis and regulation of BSi compared to fluorocarbon-based methods. Their study thoroughly investigates the impact of procedure parameters on the formation of masks and BSi creation, demonstrating that the CORE process allows for the precise manipulation of the removal and isotropic etch steps. This technique enables "BSi on demand", where the formation of BSi can be selectively controlled, offering improved uniformity across various structural dimensions and independence from the aspect ratio of the etched features. The versatility of the CORE process thus opens new avenues for applications requiring finely tuned optical and surface properties.

A plasma etching technique to fabricate BSi surfaces caped with nanoneedles altering in length, areal density, and sharpness has been employed by Hazell et al. [66]. These nanostructured surfaces were subsequently enveloped in a conformal and homogenous layer of diamond via hot filament chemical vapor deposition, thereby facilitating the formation of black diamond surfaces.

3.4. Femtosecond Laser Ablation

Direct femtosecond laser surface structuring was employed to fabricate an array of nanostructure-textured patterns on silicon substrates [67]. Xiaolong et al. created BSi using femtosecond laser pulses, focusing on minimizing charge carrier recombination caused by laser-induced damage while preserving elevated levels of absorption within the bandgap [68]. In their research, the authors conducted a comprehensive examination of the influence of laser parameters, such as focal position, average power, and scanning speed, by evaluating surface morphology, absorptance spectra, and minority carrier recombination lifetime. The results indicated that an average absorptance of approximately 96% within the visible spectrum, along with a minority carrier lifetime of 54 µs at an injection level of 1×10^{15} cm^{-3} can be attained through optimized laser parameters. These findings signify considerable progress in developing high-performance broadband optoelectronic devices utilizing surface-passivated, femtosecond-laser-processed BSi.

The BSi microfabrication process employs a variety of dry microfabrication methods to precisely define small features. It typically involves using RIE for controlled material ablation and integrating hierarchical texture and precisely sized Au NPs to achieve exceptionally low broadband reflectivity for BSi, with a reflectivity value below 1% over a wavelength range spanning 220 to 2600 nm. Additionally, using phosphorus oxychloride ($POCl_3$) and O_2 gases in RIE results in a nano-texture and superior surface roughness compared to alternative methods such as PIII and wet etching processes. Adjusting the deposition time while maintaining other parameters fixed in the DRIE leads to three distinct etching regimes. ICP-RIE etching of the BSi surface forms an effective passivation layer without the need for a separate passivation step, reducing the number of process steps. This process also allows for the production of highly curved surfaces, such as hemispherical Si lenses with a radius of 12.7 mm, resulting in significantly reduced reflectance. Furthermore, ion implantation introduces dopants into the material, creating doped Si nanowire arrays that significantly absorb light over a wide wavelength range. Plasma etching generates intricate patterns and fabricates BSi surfaces covered with nanoneedles of varying characteristics. Finally, femtosecond laser pulses are effective in achieving ultrafast and extremely accurate ablation, minimizing charge carrier recombination and preserving high bandgap absorption.

The nanostructured surface of BSi plays a pivotal role in minimizing reflectance through its anti-reflective properties and photon scattering capabilities. The surface modifications, often in the form of conical spikes or porous textures, create a graded refractive index that gradually transitions from air (~1.0) to silicon (~3.5), significantly reducing light reflection across the visible and near-infrared spectrum. This smooth transition minimizes abrupt refractive index changes that would otherwise cause light to reflect off the surface. Additionally, the rough and porous nanostructured surface promotes photon scattering, ef-

fectively extending the optical path length within the material and increasing the chances of light absorption. This mechanism can reduce reflectance to as low as 1%, as demonstrated in reactive ion etching (RIE) processed BSi surfaces [69].

The geometry of the nanostructures also plays a crucial role in enhancing light trapping. High-aspect-ratio structures, such as nanopillars and conical spikes, improve light trapping by inducing multiple internal reflections that prevent light from escaping the surface. Porous and needle-like structures further increase the surface area available for light interaction, which contributes to higher absorption efficiency. For instance, Pengfei et al. demonstrated that optimizing the roughness and aspect ratio of porous nanostructures on BSi surfaces resulted in near-perfect absorption across a broad spectrum [69].

Moreover, sub-wavelength nanostructures (with features smaller than the wavelength of light) on BSi contribute to effective light absorption by suppressing light reflection through destructive interference of reflected waves. According to the Effective Medium Theory (EMT), when surface features are much smaller than the wavelength of incident light, the material acts as an effective medium with a smoothly varying refractive index. This leads to minimal reflection and increased light absorption over a wide spectral range, making BSi highly effective in applications requiring broadband absorption [69].

Surface morphology significantly influences light-trapping efficiency. Tailoring the surface features, such as creating spiked or porous structures, enhances the material's ability to trap light at specific wavelengths, particularly in the infrared region. For example, Guanyu et al. demonstrated that Se-doped BSi surfaces, processed using laser ablation techniques, achieved broadband light absorption (400–2200 nm) by optimizing the surface morphology, resulting in improved light trapping efficiency and photodetector performance [23].

4. Black Silicon for Light Trapping in Photodetectors

Photodetectors play a crucial role in a varied range of technologies, including sensing and optical communication devices. However, typical Si-based photodetectors are constrained by their inherent limitations in light absorption, suggesting BSi as a groundbreaking solution to this challenge. As the BSi features a surface textured at the microscopic level, such a unique structure is the key to unlocking significantly improved light-trapping ability within the material. By enabling more effective light trapping, BSi-based photodetectors can achieve more excellent light absorption, leading to enhanced sensitivity and overall performance. This section discusses recent works on BSi-based photodetectors and explores the potential of BSi surfaces to improve photodetector technology.

To implement BSi and increase the performance of the photodetector, Xiaorong et al. were able to extract high peak photoresponsivity exceeding 10 A/W, as seen in Figure 4a, high optical detection, which is greater than 2×10^{12} Jones (1 Jones = 1 cm $Hz^{1/2}/W$) (see Figure 4b) through the temperature cycle (from 10 to 300 K), and broadband detection sensitivity from 400 to 1200 nm by using the femtosecond pulsed laser method to create BSi structure [70].

Moreover, the heterogeneity of the BSi layer, coupled with the presence of lattice defects, resulted in an increased noise level in devices fabricated utilizing BSi. Song et al. successfully designed and fabricated a lateral heterojunction at the interfaces of BSi and Si to mitigate leakage current [71]. Through this lateral structure, the BSi-based photodetector was able to effectively reduce dark current to 783 nA under a bias of −5 V, as presented in Figure 5, representing a substantial decrease in magnitude compared to vertical structures. Simultaneously, at the same bias voltage, they achieved a remarkable external quantum efficiency (EQE) of 371% and a photo-to-dark current ratio of 155.

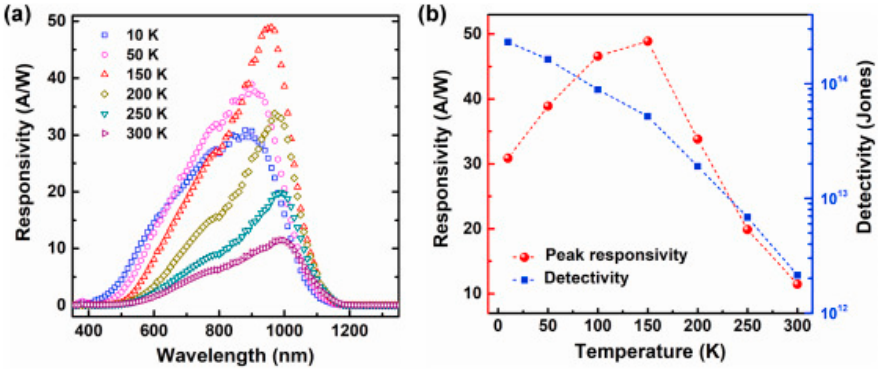

Figure 4. (**a**) Spectral responsivity of the BSi-based photodetector versus wavelength in visible and NIR regions as a function of varied temperatures from 10 K to 300 K; (**b**) the relationship between peak responsivity and detectivity in relation to temperature for the sulfur-hyper-doped BSi-based photodetector [70].

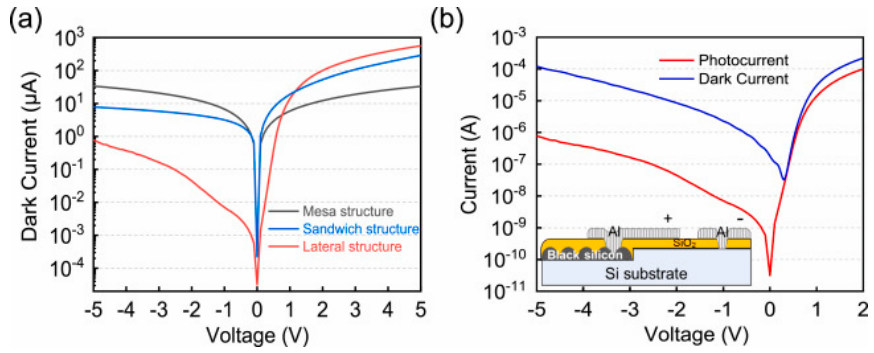

Figure 5. (**a**) Dark current features of the BSi−based photodetectors having lateral heterojunction (red line) and two vertical heterojunctions (Mesa and sandwich structures); (**b**) dark current (red line) and photocurrent (blue line) merit for the BSi−based photodetector fabricated in lateral heterojunction structure; inset presents the schematic diagram of the corresponding lateral structure of the BSi photodetector [71].

Heinonen et al. successfully conducted a comparative analysis of BSi-based photodetectors and both planar silicon-induced-junction and planar silicon-pn-junction photodetectors, with the objective of evaluating the contributions derived from the characteristics of both BSi and semiconductor junctions [72]. They assessed the EQE of all the junctions and determined that an induced junction containing BSi surface and aluminum oxide (Al_2O_3) demonstrates substantial resilience to radiation-induced proton and electron exposure degradation. While the pn-junction photodetectors, which are passivated with silicon dioxide (SiO_2), demonstrated considerable deterioration in their UV responsivity following exposure to electron irradiation. The scientific community's standard for room temperature broadband photo-response via a single device remains precedent. A variety of methodologies have been utilized in this domain, including comprehensive nanoscale patterning, the patterning and growth of heterostructures, and the modulation of band gaps through field induction. Nevertheless, the photo-response at room temperature of current photodetectors remains confined to a specific segment of the electromagnetic spectrum. Nidhi et al. successfully demonstrated the detection of broadband light in the visible to mid-infrared (MIR) range at room temperature using a lateral heterojunction-based photodetector composed of nanolayered black arsenic (BAs)-Si (BAs-Si) [73]. This broad spectral responsiveness was achieved by capitalizing on the appropriate essential band gaps of BAs and Si. Subsequently, the mechanical exfoliation technique was used to create the photodetectors of BAs on a Si-on-insulator (SOI) substrate. The device exhibited significant photo-responsivities across the visible to MIR spectrum region (405 nm to 4 μm),

attributed to the high light absorption properties of BAs and the effective optical coupling capabilities of the SOI substrate.

Chao et al. demonstrated the utilization of chromium (Cr)-hyper-doped BSi material in Si-based infrared photodetectors, exhibiting enhanced sub-bandgap absorptance and reduced ionized electron concentration [74]. The Cr-hyper-doped BSi enabled the development of BSi photodiodes with a face-to-face configuration, achieving a significant responsivity of 0.57 A/W at 1.31 μm wavelength and fast millisecond rise and delay times. Furthermore, Xiaona et al. showcased the exceptional photosensitivity properties of MSM infrared photodetectors fabricated from S-doped BSi [75]. As illustrated in Figure 6, these photodetectors demonstrated an exceptional responsivity of 367 mA/W at a voltage of 10 V, accompanied by rising and falling times of 53.82 ms and 64.51 ms, respectively, when subjected to 1030 nm laser illumination. This performance notably exceeds unprocessed Si, which exhibited a responsivity of 47 mA/W at the same voltage and under analogous experimental conditions. Furthermore, photodetectors made of two-dimensional materials (2DM PDs) can satisfy the urgent requirements of Si photonics for cost-effective, high-performance, and wide-spectrum photodetection. In Figure 6, the absorbance refers specifically to the S-doped black silicon (BSi) surface, which was processed using femtosecond laser ablation. The measurement was taken to demonstrate the intrinsic light-absorbing properties of the S-doped BSi surface, particularly in the visible to near-infrared (0.2–2.5 μm) spectrum. The data represent the effectiveness of the nanostructured BSi in minimizing light reflection while maximizing absorption across a wide range of wavelengths. The creation of micro/nanostructures on the BSi surface, formed through laser ablation, is responsible for the reduction in reflectance and enhanced absorption. These structures scatter and trap incoming light, increasing the optical path length and minimizing transmission losses. This distinction is crucial, as it highlights the performance of the S-doped BSi surface alone, without any external coatings or materials influencing the absorbance measurements. This allows for a direct comparison of the intrinsic light-trapping efficiency of the BSi nanostructures, which is key to its application in high-performance photodetectors and other optical devices that rely on efficient light absorption [72].

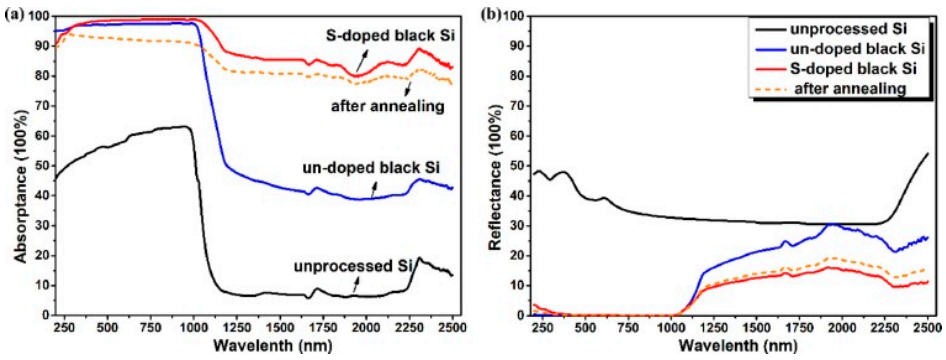

Figure 6. (**a**) Absorptance spectra as a function of wavelength spanning from 250 nm to 2500 nm and (**b**) reflectance spectra as a function of wavelength over the same range, specifically for S-doped BSi in both annealed and nonannealed states, in addition to a comparison with an undoped BSi photodetector and an unprocessed Si device [75].

Chaoyue et al. demonstrated advancements in developing Si/2DM PDs operating within the NIR to MIR wavelength range, rendering them appealing for numerous applications [76]. The use of sub-bandgap NIR Si photodetectors is essential in the domain of integrated Si photonics. In an investigation conducted by Fei Hu et al., BSi-based photodetector was successfully developed utilizing a BSi/Ag NPs Schottky junction [77]. This photodetector proficiently captures sub-bandgap light and produces a photocurrent via an amalgamation of inner photoemission, optical confinement, and surface plasmon-enhanced absorption. The BSi/Ag NPs architecture was synthesized employing a wet chemical etching process. The responsivity values of the BSi/Ag NPs photodetector demonstrated

a considerable enhancement in comparison to those of a planar-Si/Ag thin-film Schottky photodetector, achieving responsivities of 0.277 mA/W and 0.226 mA/W at a reverse bias voltage of 3 V under 1319 nm and 1550 nm light irradiation, respectively.

The Si-based photodetectors possess high detectivity and compatibility but are constrained by their low responsivity and abrupt decay when exposed to sub-bandgap wavelengths. The application of rapid thermal annealing and hydrogenated surface passivation methodologies has been observed to augment the responsivity across extensive bandgap ranges while improving the signal-to-noise ratio of photodetectors. The photodetector exhibits a sub-bandgap responsivity of 0.80 A/W at a voltage of less than 20 V for a wavelength of 1550 nm and an outstanding responsivity of 1097.60 A/W for a wavelength of 1080 nm. These characteristics underscore its potential competitiveness in fields such as infrared light detection, night vision imaging, and fiber-optic communication [78]. A recent study examined broadband BSi-based photodetectors characterized by high comprehensive properties and significant spectral responsivity [79]. These devices demonstrate responsiveness to incident light ranging from 400 nm to 1550 nm, as illustrated in Figure 7, and exhibit a notable responsivity of 40.59 A/W at 950 nm under a bias of −5 V. The produced photodetector reveals a consistent sub-bandgap photocurrent at 1550 nm. The hyper-doping of titanium (Ti) within Si enhances its efficacy, providing valuable implications for optical applications such as the detection of weak and infrared photons.

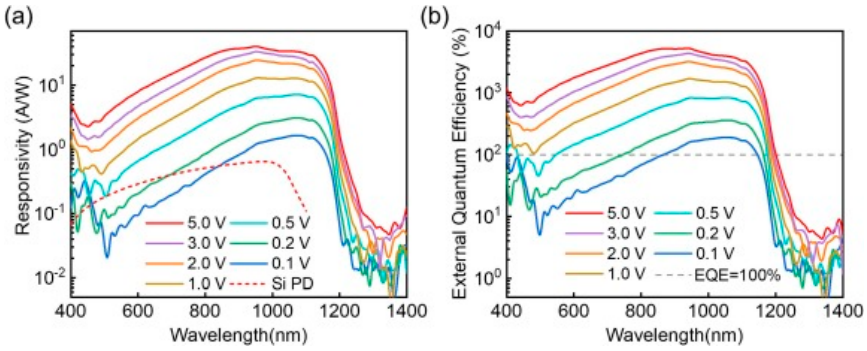

Figure 7. Responsivity characteristics of the optimized Ti hyper-doped BSi photodetector, illustrating (**a**) the responsivity under various bias voltages; the red dotted line denotes the responsivity of a commercial silicon photodiode (Si PD) under a bias voltage of −12 V for comparative purposes; (**b**) the corresponding EQE of the titanium hyper-doped BSi photodetector is depicted, with the dotted gray line indicating an EQE value of 100% [79].

The importance of photodetectors in various technologies, such as optical communication devices and sensors, cannot be overstated. However, the limitations of Si-based photodetectors hinder their light-detection capabilities, which is where BSi comes in as a groundbreaking solution. The microscopically textured surface of BSi plays a crucial role in enhancing its light-trapping capabilities, allowing BSi-based photodetectors to achieve improved light absorption and overall performance. By implementing BSi in the photodetector, significant improvements have been achieved, including high peak photoresponsivity, reduced current leakage, enhanced photocurrent rate, and remarkable EQE value. Additionally, photodetectors based on BSi exhibit enhanced sub-bandgap absorptance, reduced ionized electron concentration, and fast millisecond rise and delay times. Furthermore, BSi-based photodetectors address key challenges faced by photodetector devices, including low responsivity and abrupt decay when exposed to sub-bandgap wavelengths. This objective is accomplished through the application of rapid thermal annealing and hydrogenated surface passivation techniques in conjunction with BSi, which collectively enhance broadband spectral responsivity, yield high gain, and improve the signal-to-noise ratio of the photodetectors. Table 2 illustrates a concise overview of the recent BSi-based photodetectors to achieve enhanced functionalities and address the existing limitations of these optical devices.

Table 2. A summary of the recent works in BSi-based photodetectors to enhance functionalities and address Si-based photodetectors' limitations.

Study Objectives	Methodologies	Results	Applications	Ref.
Studying the properties of temperature-dependent photodetection of sulfur-hyper-doped Si from 10 to 300 K	Fabricated by femtosecond laser	The subject exhibits a peak photoresponsivity that surpasses 10 A/W, a notably elevated specific detectivity exceeding 2×10^{12} Jones across the temperature spectrum, and a broad detection sensitivity ranging from 400 to 1200 nm. Furthermore, the interaction between femtosecond laser pulses and Si occurs with remarkable rapidity, generating hyper-doped carriers at multiple sub-bandgap energy levels, thereby facilitating substantial carrier activity within the temperature range of 10 to 300 K.	Multifunctional optoelectronic devices	[70]
To decrease high noise	By fabricating a lateral heterojunction	The suppression of the dark current to 783 nA at a bias of −5 volts is notably low compared to the vertical configurations in terms of orders of magnitude, while the external quantum efficiency is recorded at 371%.	Massive integration in optical-electronic systems or flip–chip interconnection frameworks	[71]
To study the stability of BSi-induced junction photodetectors under high-energy irradiation	By comparing the planar Si-induced junction and the planar Si-pn-junction photodetectors	The integration of the BSi surface and Al_2O_3-induced junction demonstrates considerable resistance to radiation when exposed to the utilized proton and electron dosages, revealing deterioration solely in the NIR region. Conversely, applying SiO_2 passivation results in a marked decline in ultraviolet responsivity.	Space applications	[72]
Widen the light band from one single bandwidth to broadband.	Using a lateral heterojunction-based photodetector composed of nanolayered BAs-Si	The observed photo-responsivities exhibit significant values across the visible to MIR spectrum, specifically within the wavelength range of 405 nm to 4 µm. The maximal photo-responsivity measurements recorded are 72.15 A/W, 930.49 A/W, and 75.2 A/W at wavelengths of 785 nm, 1.05 µm, and 3 µm, respectively. Correspondingly, the maximum detectivities are quantified as 3.2 × 109, 4.17 × 1010, and 3.37 × 109 Jones, respectively. Furthermore, the system can detect weak optical signals and demonstrates a degree of sensitivity to the polarization of incident radiation.	BAs present a potential avenue for actualizing SOI technology that is applicable across a diverse spectrum	[73]
To enhance the sub-bandgap absorptance and reduce the ionized electron concentration	By Cr-hyper-doped BSi material in Si-based infrared photodetectors	The BSi layer contains Cr atoms exceeding 1020 cm^{-3}, resulting in a large sub-bandgap absorptance of approximately 60% for 1.31 µm. The Cr impurity introduces a deep-energy level 0.39 eV below the conduction band bottom, resulting in a very low ionized electron concentration (~1015 cm^{-3}). 0.57 A/W of responsivity under 1.31 µm light illumination, with a millisecond rise and delay time to infrared light.	communication wavebands	[74]
To achieve elevated absorption across an extensive spectral range, encompassing visible to infrared wavelengths.	Using femtosecond laser irradiation in ambient air	Superior infrared absorption under its bandgap, with an absorptance exceeding 85% ranging from 0.2 to 2.5 µm.	Optoelectronic devices.	[75]

Table 2. *Cont.*

Study Objectives	Methodologies	Results	Applications	Ref.
Reviewing recent progress in Si/2DM photodetectors	By focusing on the ultrabroad operation wavelength range and flexible integration, particularly in the NIR to MIR wavelength band	Significant advancements have been realized, encompassing approximately 100 GHz high-bandwidth M-G-M PDs. Photodetectors based on the ultra-high sensitivity of the PG effect. A number of representative wafer-scale image sensors constructed from Si/2DM PDs, along with their corresponding arrays, have also been demonstrated. The 2DM PDs fulfill the pressing requirements of silicon photonics through their cost-effectiveness, high performance, and broadband photodetection capabilities.	Integrating 2DMs with Si microelectronics and photonics presents a compelling technological pathway for developing high-performance, cost-effective PDs, which may significantly influence the advancement of next-generation optoelectronic integrated circuits.	[76]
To enhance the capturing of the sub-bandgap light and create a photocurrent	By preparing Si photodetector based on a BSi/Ag NPs Schottky junction	The BSi/Ag NPs photodetector demonstrated significantly improved responsivities compared to a planar-Si/Ag thin-film Schottky photodetector and demonstrates responsivity values of 0.277 mA/W and 0.226 mA/W at a voltage of 3 V for light wavelengths of 1319 nm and 1550 nm, respectively.	Integrated Si photonics	[77]
To enhance the responsivity of wide-bandgap semiconductors and improve the signal-to-noise ratio while minimizing the dark current	By utilizing rapid thermal annealing and hydrogenated surface passivation were used	A notable sub-bandgap responsivity of 0.80 A/W was observed for a wavelength of 1550 nm at an applied voltage of 20 V under ambient temperature conditions. Using the 400–1700 nm spectral range, the highest responsivity at 1080 nm was 1097.60 A/W under 20 V. The detectivity exhibited is remarkably high (1.22 × 1014 Jones at −5 V), attributable to the application of post-processing techniques and a reduction in dark current, measured at 7.8 μA under −5 V.	- In integration with photonics and electronics (IR light detection, night vision imaging, and fiber-optic communication). - Enhancing the development of energy devices, information technology, and artificial intelligence.	[78]
To introduce a highly comprehensive BSi photodetector characterized by broadband spectral responsivity and elevated gain.	Via using hyper-doping of Ti in Si of the BSi photodetector	The response to incident light ranges from 400 nm to 1550 nm. A notable responsivity of 40.59 A/W was observed at a wavelength of 950 nm under a bias of −5 V. A consistent sub-bandgap photocurrent at a wavelength of 1550 nm.	Optoelectronic devices	[79]

Silver-assisted metal-assisted chemical etching (Ag-MACE) significantly improved the performance of multi-crystalline silicon-based photodetectors. Li et al. demonstrated that the average responsivity of photodetectors with Ag-MACE-modified BSi surfaces substantially increased from 0.64 A/W to 19.24 A/W, largely due to optimized surface nanostructures, which enhanced light trapping and reduced reflectance [24]. In another study, reactive ion etching (RIE) produced hierarchical micro/nanostructures that reduced reflectance to less than 1% across the visible and near-infrared (NIR) spectrum. François et al. reported that such structures enhanced the quantum efficiency (QE) of photodetectors to 99% in the visible range, while significantly reducing noise levels [51].

Deep reactive ion etching (DRIE), which forms deep nanostructures, has demonstrated high responsivity values. For instance, BSi photodetectors fabricated through DRIE showed excellent responsivity of up to 40 A/W at 950 nm, with a noise equivalent power (NEP) of 10–14 W/Hz0.5 [54]. Moreover, laser ablation has been employed to enhance photodetector performance, particularly in the infrared region. Guanyu et al. demonstrated that Se-doped BSi photodetectors, created using laser ablation, exhibited broadband absorption from 400 nm to 2200 nm. These photodetectors reached a peak quantum efficiency of 96%, with a responsivity exceeding 10 A/W in the near-infrared range, and reduced dark current to below 783 nA at a bias of −5 V [23].

Table 3 presents a comparative analysis focused on critical metrics: light absorption efficiency, fabrication cost, process complexity, and scalability to provide clearer insights into the advantages and disadvantages of various BSi surface modification techniques.

Each technique offers distinct benefits and trade-offs, making them more or less suitable for different applications. In addition, each technique offers specific advantages depending on the application. For instance, MACE is highly scalable and cost-effective, making it suitable for large-scale photovoltaic cell production. In contrast, RIE and DRIE provide more precise control over surface structures but come with higher complexity and cost. Techniques like electrochemical etching offer a balance of efficiency and simplicity, while laser ablation is ideal for applications requiring highly tailored surface morphologies.

Table 3. Comparative analysis of BSi surface modification techniques.

Method	Light Absorption Efficiency	Fabrication Cost	Complexity	Scalability	Reference
Metal-Assisted Chemical Etching (MACE)	High (can achieve >90% light absorption)	Low (uses common chemicals like Ag, Cu)	Moderate (dependent on control over nanoparticle formation)	High (scalable for large surfaces, suitable for industrial use)	[24–27]
Reactive Ion Etching (RIE)	Very High (<1% reflectance over a broad range)	Moderate (requires specific gas setups)	High (requires precise control of etching parameters)	Medium (limited scalability due to equipment needs)	[50–53]
Electrochemical Etching	High (1% reflectance in the visible spectrum)	Low (inexpensive setup)	Low (simpler than RIE or DRIE)	Medium (scalability depends on etching uniformity)	[40,41]
Deep Reactive Ion Etching (DRIE)	Very High (nanopillars enhance absorption)	High (requires advanced machinery)	Very High (complex cyclic process)	Low (best suited for specialized applications)	[54,55]
Laser Ablation	High (can tailor absorption for specific wavelengths)	Moderate (cost of laser systems)	Moderate (requires precise laser control)	Medium (suitable for patterning small areas)	[65,66]

5. Conclusions

In conclusion, this work offers an extensive evaluation of recent advancements in the physical and chemical processing of BSi, emphasizing the potential of BSi structures for effectively trapping light in high-performance photodetectors. The recent work on BSi processing methods, including metal-assisted chemical etching, electrochemical etching, reactive ion etching, plasma etching, and laser ablation are reviewed with a keen interest in the resulting BSi micro- and nanostructures. Particularly, Ag-assisted MACE has demonstrated substantial performance improvements in broadband light absorption and reflectivity reduction, as observed in studies showing that this method substantially enhanced the efficiency of multi-crystalline BSi solar cells from 0.64% to 19.24% [24]. This review not only builds upon the foundational work of previous scholars but also presents our own contributions in the field of BSi fabrication. It delves deeply into the critical aspects of micro- and nanofabrication of BSi, offering an in-depth exploration of how a wide variety of processing techniques impact BSi. In addition, RIE and DRIE methods have shown the ability to create high-aspect-ratio nanostructures that reduce reflectance to as low as 1% and significantly enhance quantum efficiency, achieving up to 99% in some design cases [51]. On the other hand, laser ablation, particularly Se-doped BSi structures, has demonstrated remarkable broadband absorption (400–2200 nm), making it a viable method for advanced photodetectors with improved broadband responsivity [23]. This thorough investigation sets the stage for future developments in surface modification strategies for Si-based optical devices, particularly microstructures. Ultimately, the recent findings and implementations of BSi-based photodetectors are discussed. By optimizing BSi processing for light trapping, the potential of this material's properties in light trapping could pave the way for next-generation photodetectors with enhanced sensitivity and responsivity. Finally, while the methods reviewed in this manuscript such as metal-assisted chemical etching

(MACE), reactive ion etching (RIE), and laser ablation have been primarily applied to rigid photodetectors, their adaptation for flexible photodetectors holds potential. Challenges such as maintaining structural integrity during bending and ensuring uniform nanostructure formation on flexible substrates remain, but advancements in material science and fabrication techniques could enable the use of BSi in flexible optoelectronic devices in the future. Looking ahead, one of the most promising prospects in this field is the integration of BSi with other materials, such as plasmonic nanoparticles or quantum dots, to further enhance light trapping and detection capabilities. However, significant challenges remain, particularly in scaling these techniques for industrial applications. Uniformity of nanostructures over large areas, cost-effective fabrication, and the durability of BSi in varying environmental conditions are critical issues that must be addressed. Additionally, optimizing BSi processing for flexible substrates presents an important future challenge, as the transition from rigid to flexible devices will require overcoming issues like nanostructure adhesion and mechanical stability.

Funding: This article is derived from a research grant funded by the Research, Development, and Innovation Authority (RDIA)—Kingdom of Saudi Arabia—with grant number (12870-KACST-2023-KACST-R-2-1-EI-).

Acknowledgments: The authors would like to express their sincere appreciation for the ongoing and invaluable support provided by King Abdulaziz City for Science and Technology (KACST). Additionally, the authors would like to acknowledge Aljoharah Alabdan for her work in collecting chemical etching references.

Conflicts of Interest: The authors declare no conflicts of interest.

References

1. Saab, D.A.; Basset, P.; Pierotti, M.J.; Trawick, M.L.; Angelescu, D.E. Static and dynamic aspects of black silicon formation. *Phys. Rev. Lett.* **2014**, *113*, 265502. [CrossRef] [PubMed]
2. Tan, X.; Tao, Z.; Yu, M.; Wu, H.; Li, H. Anti-reflectance optimization of secondary nanostructured black silicon grown on micro-structured arrays. *Micromachines* **2018**, *9*, 385. [CrossRef] [PubMed]
3. Zhang, Z.; Wang, Y.; Hansen, P.A.S.; Du, K.; Gustavsen, K.R.; Liu, G.; Karlsen, F.; Nilsen, O.; Xue, C.; Wang, K. Black silicon with order-disordered structures for enhanced light trapping and photothermic conversion. *Nano Energy* **2019**, *65*, 103992. [CrossRef]
4. Teo, A.L.; Shearwood, C.; Ng, K.C.; Lu, J.; Moochhala, S. Transdermal microneedles for drug delivery applications. *Mater. Sci. Eng. B* **2006**, *132*, 151–154. [CrossRef]
5. Langer, C.; Prommesberger, C.; Ławrowski, R.; Schreiner, R.; Serbun, P.; Müller, G.; Düsberg, F.; Hofmann, M.; Bachmann, M.; Pahlke, A. Field emission properties of p-type black silicon on pillar structures. *J. Vac. Sci. Technol. B* **2016**, *34*, 02G107. [CrossRef]
6. Zhong, S.; Liu, B.; Xia, Y.; Liu, J.; Liu, J.; Shen, Z.; Xu, Z.; Li, C. Influence of the texturing structure on the properties of black silicon solar cell. *Sol. Energy Mater. Sol. Cells* **2013**, *108*, 200–204. [CrossRef]
7. Scheul, T.E.; Khorani, E.; Rahman, T.; Charlton, M.D.; Boden, S.A. Light scattering from black silicon surfaces and its benefits for encapsulated solar cells. *Sol. Energy Mater. Sol. Cells* **2022**, *235*, 111448. [CrossRef]
8. Jia, Z.; Wu, Q.; Jin, X.; Huang, S.; Li, J.; Yang, M.; Huang, H.; Yao, J.; Xu, J. Highly responsive tellurium-hyperdoped black silicon photodiode with single-crystalline and uniform surface microstructure. *Opt. Express* **2020**, *28*, 5239–5247. [CrossRef]
9. Tyson, J.J.; Scheul, T.E.; Rahman, T.; Boden, S.A. Characterising the broadband, wide–angle reflectance properties of black silicon surfaces for photovoltaic applications. *Opt. Express* **2023**, *31*, 28295–28307. [CrossRef]
10. Jansen, H.; De Boer, M.; Legtenberg, R.; Elwenspoek, M. The black silicon method: A universal method for determining the parameter setting of a fluorine-based reactive ion etcher in deep silicon trench etching with profile control. *J. Micromech. Microeng.* **1995**, *5*, 115–120. [CrossRef]
11. Her, T.-H.; Finlay, R.J.; Wu, C.; Deliwala, S.; Mazur, E. Microstructuring of silicon with femtosecond laser pulses. *Appl. Phys. Lett.* **1998**, *73*, 1673–1675. [CrossRef]
12. Mokkapati, S.; Catchpole, K.R. Nanophotonic light trapping in solar cells. *J. Appl. Phys.* **2012**, *112*, 101101. [CrossRef]
13. Niu, C.; Zhu, T.; Lv, Y. Influence of Surface Morphology on Absorptivity of Light-Absorbing Materials. *Int. J. Photoenergy* **2019**, *2019*, 1–9. [CrossRef]
14. Southwell, W.H. Pyramid-array surface-relief structures producing antireflection index matching on optical surfaces. *J. Opt. Soc. Am. A* **1991**, *8*, 549–553. [CrossRef]
15. Hobbs, D.S.; MacLeod, B.D.; Riccobono, J.R. Update on the development of high performance anti-reflecting surface relief micro-structures. In *Window and Dome Technologies and Materials X*; SPIE: Bellingham, WA, USA, 2007; Volume 6545, pp. 242–255. [CrossRef]

16. Kolasinski, K.W. Silicon nanostructures from electroless electrochemical etching. *Curr. Opin. Solid State Mater. Sci.* **2005**, *9*, 73–83. [CrossRef]
17. Liu, X.; Radfar, B.; Chen, K.; Setala, O.E.; Pasanen, T.P.; Yli-Koski, M.; Savin, H.; Vähänissi, V. Perspectives on Black Silicon in Semiconductor Manufacturing: Experimental Comparison of Plasma Etching, MACE, and Fs-Laser Etching. *IEEE Trans. Semicond. Manuf.* **2022**, *35*, 504–510. [CrossRef]
18. Tan, X.; Tao, Z.; Yu, M.; Wu, H.; Li, H. Anti-reflectance investigation of a micro-nano hybrid structure fabricated by dry/wet etching methods. *Sci. Rep.* **2018**, *8*, 7863. [CrossRef]
19. Koynov, S.; Brandt, M.S.; Stutzmann, M. Black thin film silicon. *J. Appl. Phys.* **2011**, *110*, 043537. [CrossRef]
20. Ma, S.; Liu, S.; Xu, Q.; Xu, J.; Lu, R.; Liu, Y.; Zhong, Z. A theoretical study on the optical properties of black silicon. *AIP Adv.* **2018**, *8*, 35010. [CrossRef]
21. Ayvazyan, G.Y. Modelling of the Porous and Black Silicon Reflection Characteristics. *J. Contemp. Phys.* **2023**, *58*, 164–171. [CrossRef]
22. Cheng, P.; Wang, H.; Müller, B.; Müller, J.; Wang, D.; Schaaf, P. Photo-Thermoelectric Conversion Using Black Silicon with Enhanced Light Trapping Performance far beyond the Band Edge Absorption. *ACS Appl. Mater. Interfaces* **2021**, *13*, 1818–1826. [CrossRef] [PubMed]
23. Mi, G.; Lv, J.; Que, L.; Zhang, Y.; Zhou, Y.; Liu, Z. A Dual Four-Quadrant Photodetector Based on Near-Infrared Enhanced Nanometer Black Silicon. *Nanoscale Res. Lett.* **2021**, *16*, 38. [CrossRef] [PubMed]
24. Li, X.; Gao, Z.; Zhang, D.; Tao, K.; Jia, R.; Jiang, S.; Wang, B.; Ji, Z.; Jin, Z.; Liu, X. High-efficiency multi-crystalline black silicon solar cells achieved by additive assisted Ag-MACE. *Sol. Energy* **2020**, *195*, 176–184. [CrossRef]
25. Noor, N.A.M.; Mohamad, S.K.; Hamil, S.S.; Devarajan, M.; Pakhuruddin, M.Z. Effects of etching time towards broadband absorption enhancement in black silicon fabricated by silver-assisted chemical etching. *Optik* **2019**, *176*, 586–592. [CrossRef]
26. Abdulkadir, A.; Aziz, A.b.A.; Pakhuruddin, M.Z. Optimization of etching time for broadband absorption enhancement in black silicon fabricated by one-step electroless silver-assisted wet chemical etching. *Optik* **2019**, *187*, 74–80. [CrossRef]
27. Venkatesan, R.; Arivalagan, M.K.; Venkatachalapathy, V.; Pearce, J.M.; Mayandi, J. Effects of silver catalyst concentration in metal assisted chemical etching of silicon. *Mater. Lett.* **2018**, *221*, 206–210. [CrossRef]
28. Abdulkadir, A.; Isiyaku, A.K.; Isah, M.; Abbas, D.U.; Ismaila, T. Effect of sputtered silver thin film thickness towards morphological and optical properties of black silicon fabricated by two-step silver-assisted wet chemical etching for solar cells application. *Phys. Access* **2022**, *2*, 70–77. [CrossRef]
29. Tang, Q.; Shen, H.; Yao, H.; Jiang, Y.; Li, Y.; Zhang, L.; Ni, Z.; Wei, Q. Formation mechanism of inverted pyramid from sub-micro to micro scale on c-Si surface by metal assisted chemical etching temperature. *Appl. Surf. Sci.* **2018**, *455*, 283–294. [CrossRef]
30. Li, P.; Wei, Y.; Zhao, Z.; Tan, X.; Bian, J.; Wang, Y.; Lu, C.; Liu, A. Highly efficient industrial large-area black silicon solar cells achieved by surface nanostructured modification. *Appl. Surf. Sci.* **2015**, *357*, 1830–1835. [CrossRef]
31. Park, J.E.; Cho, Y.H.; Kang, S.; Hong, H.K.; Kim, D.S.; Lim, D. Effect of Cu-Assisted Chemical Etching for Black Silicon. In Proceedings of the 2018 IEEE 7th World Conference on Photovoltaic Energy Conversion, WCPEC 2018—A Joint Conference of 45th IEEE PVSC, 28th PVSEC and 34th EU PVSEC, Waikoloa, HI, USA, 10–15 June 2018; pp. 1047–1050. [CrossRef]
32. Zhao, Y.; Liu, Y.; Chen, W.; Wu, J.; Chen, Q.; Tang, H.; Wang, Y.; Du, X. Regulation of surface texturization through copper-assisted chemical etching for silicon solar cells. *Sol. Energy* **2020**, *201*, 461–468. [CrossRef]
33. Volovlikova, O.V.; Gavrilov, S.; Lazarenko, P.; Kukin, A.; Dudin, A.; Tarhanov, A. Influence of Etching Regimes on the Reflectance of Black Silicon Films Formed by Ni-Assisted Chemical Etching. *Key Eng. Mater.* **2019**, *806*, 24–29. [CrossRef]
34. Arafat, M.Y.; Islam, M.A.; Bin Mahmood, A.W.; Abdullah, F.; Nur-E-Alam, M.; Kiong, T.S.; Amin, N. Fabrication of Black Silicon via Metal-Assisted Chemical Etching—A Review. *Sustainability* **2021**, *13*, 10766. [CrossRef]
35. Uddin, S.; Hashim, M.R.; Pakhuruddin, M.Z. Influence of Catalyst Thickness and Etching Solution Composition on Properties of Black Silicon Fabricated Via Aluminium-Assisted Chemical Etching. *SSRN* **2022**. [CrossRef]
36. Uddin, S.; Hashim, R.; Pakhuruddin, M.Z. Aluminium-assisted chemical etching for fabrication of black silicon. *Mater. Chem. Phys.* **2021**, *265*, 124469. [CrossRef]
37. Uddin, S.; Hashim, M.; Pakhuruddin, M.Z. Effects of annealing temperature towards properties of black silicon fabricated by aluminium-assisted chemical etching. *Mater. Sci. Semicond. Process.* **2021**, *133*, 105932. [CrossRef]
38. Ibrahim, I.M.; Noori, Z.M.; Hwail, H.M.; Abdullah, M.M. Morphological and Optical Study of Black P- Silicon Textured in KOH Bath. *Diffus. Found. Mater. Appl.* **2023**, *32*, 35–43. [CrossRef]
39. Arafat, Y.; Islam, M.A.; Bin Mahmood, A.W.; Abdullah, F.; Kiong, T.S.; Amin, N. Study of Black Silicon Wafer through Wet Chemical Etching for Parametric Optimization in Enhancing Solar Cell Performance by PC1D Numerical Simulation. *Crystals* **2021**, *11*, 881. [CrossRef]
40. Zhong, F.; Mo, J.; Li, Y.; Sun, B.; Wu, Z. Optical characteristics of porous silicon photonic crystals prepared on the back surface of silicon wafers. *Optik* **2020**, *201*, 163486. [CrossRef]
41. Hwail, H.M.; Abdullah, M.M. Implementation of P-type black silicon with high aspect ratio for optoelectronics applications. *EUREKA Phys. Eng.* **2021**, *4*, 134–140. [CrossRef]
42. Tang, Y.; Li, R.; Sun, R.; Min, J.; Lin, Q.; Yang, C.; Xie, G. Flexible all-organic photodetectors via universal water-assisted transfer printing. *Innovation* **2023**, *4*, 100460. [CrossRef]

43. Fei, W.; Wu, Z.; Cheng, H.; Xiong, Y.; Chen, W.; Meng, L. Molecular mobility and morphology change of poly(vinyl alcohol) (PVA) film as induced by plasticizer glycerol. *J. Polym. Sci.* **2023**, *61*, 1959–1970. [CrossRef]
44. Hsu, C.-H.; Liu, S.-M.; Wu, W.-Y.; Cho, Y.-S.; Huang, P.-H.; Huang, C.-J.; Lien, S.-Y.; Zhu, W.-Z. Nanostructured pyramidal black silicon with ultra-low reflectance and high passivation. *Arab. J. Chem.* **2020**, *13*, 8239–8247. [CrossRef]
45. Sreejith, K.P.; Sharma, A.K.; Behera, S.; Kumbhar, S.; Basu, P.; Kottantharayil, A. Optimization of MACE black silicon surface morphology in multi-crystalline wafers for excellent opto-electronic properties. In Proceedings of the 2020 47th IEEE Photovoltaic Specialists Conference (PVSC), Calgary, AB, Canada, 15 June 2020; pp. 839–842. [CrossRef]
46. Chen, K.; Pasanen, T.P.; Vahanissi, V.; Savin, H. Effect of MACE Parameters on Electrical and Optical Properties of ALD Passivated Black Silicon. *IEEE J. Photovolt.* **2019**, *9*, 974–979. [CrossRef]
47. Ray, S.; Mondal, A.; Gangopadhyay, U. Optimization and characterization of silicon nano-grass antireflection layer on textured silicon wafer. *Appl. Phys. A* **2020**, *126*, 399. [CrossRef]
48. Meng, Y.; An, L.; Han, X.; Li, Y.; Hou, C.; Zhang, Q.; Wang, H. Controllable (Ga1−xZnx)(N1−xOx) nanorods grown on black silicon as anodes for water splitting. *Appl. Surf. Sci.* **2020**, *502*, 144174. [CrossRef]
49. Gao, K.; Shen, H.; Liu, Y.; Jiang, Y.; Zheng, C.; Li, Y.; Ren, S.; Huang, C. Enhanced etching rate of black silicon by Cu/Ni Co-assisted chemical etching process. *Mater. Sci. Semicond. Process.* **2018**, *88*, 250–255. [CrossRef]
50. Putra, I.R.; Li, J.-Y.; Chen, C.-Y. 18.78% hierarchical black silicon solar cells achieved with the balance of light-trapping and interfacial contact. *Appl. Surf. Sci.* **2019**, *478*, 725–732. [CrossRef]
51. Ghezzi, F.; Pedroni, M.; Kovač, J.; Causa, F.; Cremona, A.; Anderle, M.; Caniello, R.; Pietralunga, S.M.; Vassallo, E. Unraveling the Mechanism of Maskless Nanopatterning of Black Silicon by CF_4/H_2 Plasma Reactive-Ion Etching. *ACS Omega* **2022**, *7*, 25600–25612. [CrossRef]
52. Zhang, Z.; Martinsen, T.; Liu, G.; Tayyib, M.; Cui, D.; de Boer, M.J.; Karlsen, F.; Jakobsen, H.; Xue, C.; Wang, K. Ultralow Broadband Reflectivity in Black Silicon via Synergy between Hierarchical Texture and Specific-Size Au Nanoparticles. *Adv. Opt. Mater.* **2020**, *8*, 2000668. [CrossRef]
53. Atteia, F.; Le Rouzo, J.; Denaix, L.; Duché, D.; Berginc, G.; Simon, J.J.; Escoubas, L. Morphologies and optical properties of black silicon by room temperature reactive ion etching. *Mater. Res. Bull.* **2020**, *131*, 110973. [CrossRef]
54. Fung, T.H.; Pasanen, T.P.; Zhang, Y.; Soeriyadi, A.; Vähänissi, V.; Scardera, G.; Payne, D.; Savin, H.; Abbott, M. Improved emitter performance of RIE black silicon through the application of in-situ oxidation during POCl3 diffusion. *Sol. Energy Mater. Sol. Cells* **2020**, *210*, 110480. [CrossRef]
55. Nm, R.; Banobre, A.; Marthi, S.R. Atomic force microscopy studies of formation of black silicon by reactive ion etching. *Mater. Sci. Eng. Int. J.* **2018**, *2*, 134–137. [CrossRef]
56. Yusuf, M.; Herring, G.K.; Neustock, L.T.; Zaman, M.A.; Raghuram, U.; Narasimhan, V.K.; Chia, C.; Howe, R.T. Optimized Deep Reactive-Ion Etching of Nanostructured Black Silicon for High-Contrast Optical Alignment Marks. *ACS Appl. Nano Mater.* **2021**, *4*, 7047–7061. [CrossRef]
57. Zaman, A. Hybrid RF Acoustic Resonators and Arrays with Integrated Capacitive and Piezoelectric Transducers. Ph.D. Thesis, University of South Florida, Tampa, FL, USA, 2020.
58. Schmelz, D.; Käsebier, T.; Shi, Z.; Cheng, Q.; Sergeev, N.; Schelle, D.; Zeitner, U. Investigations on black silicon nanostructures fabricated by reactive ion etching on highly curved surfaces. *Mater. Sci. Semicond. Process.* **2023**, *165*, 107646. [CrossRef]
59. Zhang, Y. Advanced Characterisation of Black Silicon by Electron Microscopy Techniques. Ph.D. Thesis, The University of New South Wales, Sydney, Australia, 2022. [CrossRef]
60. Alsolami, A.; Zaman, A.; Rivera, I.F.; Baghelani, M.; Wang, J. Improvement of deep reactive ion etching process for motional resistance reduction of capacitively transduced vibrating resonators. *IEEE Sens. Lett.* **2018**, *2*, 1–4. [CrossRef]
61. Fan, Z.; Cui, D.; Zhang, Z.; Zhao, Z.; Chen, H.; Fan, Y.; Li, P.; Zhang, Z.; Xue, C.; Yan, S. Recent Progress of Black Silicon: From Fabrications to Applications. *Nanomaterials* **2021**, *11*, 41. [CrossRef]
62. Liu, K.; Qu, S.; Zhang, X.; Tan, F.; Bi, Y.; Lu, S.; Wang, Z. Sulfur-doped black silicon formed by metal-assist chemical etching and ion implanting. *Appl. Phys. A* **2014**, *114*, 765–768. [CrossRef]
63. Xiao, G.; Liu, B.; Liu, J.; Xu, Z. The study of defect removal etching of black silicon for solar cells. *Mater. Sci. Semicond. Process.* **2014**, *22*, 64–68. [CrossRef]
64. Lanterne, A.; Desrues, T.; Lorfeuvre, C.; Coig, M.; Torregrosa, F.; Milési, F.; Roux, L.; Dubois, S. Plasma-immersion ion implantation: A path to lower the annealing temperature of implanted boron emitters and simplify PERT solar cell processing. *Prog. Photovolt. Res. Appl.* **2019**, *27*, 1081–1091. [CrossRef]
65. Nguyen, V.T.H.; Jensen, F.; Hübner, J.; Leussink, P.; Jansen, H. On the formation of black silicon in SF6-O2 plasma: The clear, oxidize, remove, and etch (CORE) sequence and black silicon on demand. *J. Vac. Sci. Technol. A Vac. Surf. Film.* **2020**, *38*, 043004. [CrossRef]
66. Hazell, G.; May, P.W.; Taylor, P.; Nobbs, A.H.; Welch, C.C.; Su, B. Studies of black silicon and black diamond as materials for antibacterial surfaces. *Biomater. Sci.* **2018**, *6*, 1424–1432. [CrossRef] [PubMed]
67. Vorobyev, A.; Guo, C. Direct creation of black silicon using femtosecond laser pulses. *Appl. Surf. Sci.* **2011**, *257*, 7291–7294. [CrossRef]

68. Liu, X.; Radfar, B.; Chen, K.; Pasanen, T.P.; Vähänissi, V.; Savin, H. Tailoring Femtosecond-Laser Processed Black Silicon for Reduced Carrier Recombination Combined with >95% Above-Bandgap Absorption. *Adv. Photonics Res.* **2022**, *3*, 2100234. [CrossRef]
69. Zhang, P.; Li, S.; Liu, C.; Wei, X.; Wu, Z.; Jiang, Y.; Chen, Z. Near-infrared optical absorption enhanced in black silicon via Ag nanoparticle-induced localized surface plasmon. *Nanoscale Res. Lett.* **2014**, *9*, 519. [CrossRef] [PubMed]
70. Jin, X.; Wu, Q.; Huang, S.; Deng, G.; Yao, J.; Huang, H.; Zhao, P.; Xu, J. High-performance black silicon photodetectors operating over a wide temperature range. *Opt. Mater.* **2021**, *113*, 110874. [CrossRef]
71. Huang, S.; Deng, G.; Jin, X.; Lu, Y.; Song, G.; Huang, H.; Zhao, P.; Zhang, C.; Yao, J.; Wu, Q.; et al. The dark current suppression of black silicon photodetector by a lateral heterojunction. *Opt. Mater.* **2020**, *110*, 110474. [CrossRef]
72. Heinonen, J.; Modanese, C.; Haarahiltunen, A.; Kettunen, H.; Rossi, M.; Jaatinen, J.; Juntunen, M. Results on radiation hardness of black silicon induced junction photodetectors from proton and electron radiation. *Nucl. Instrum. Methods Phys. Res. Sect. A* **2020**, *977*, 164294. [CrossRef]
73. Nidhi; Jakhar, A.; Uddin, W.; Kumar, J.; Nautiyal, T.; Das, S. Nanolayered Black Arsenic–Silicon Lateral Heterojunction Photodetector for Visible to Mid-Infrared Wavelengths. *ACS Appl. Nano Mater.* **2020**, *3*, 9401–9409. [CrossRef]
74. Li, C.; Zhao, J.-H.; Yang, Y.; Chen, Q.-D.; Chen, Z.-G.; Sun, H.-B. Sub-bandgap photo-response of chromium hyperdoped black silicon photodetector fabricated by femtosecond laser pulses. *IEEE Sens. J.* **2021**, *21*, 25695–25702. [CrossRef]
75. Zhao, X.; Lin, K.; Zhao, B.; Du, W.; Nivas, J.J.; Amoruso, S.; Wang, X. Broadband MSM photodetector based on S-doped black silicon fabricated by femtosecond laser. *Appl. Surf. Sci.* **2023**, *619*, 156624. [CrossRef]
76. Liu, C.; Guo, J.; Yu, L.; Li, J.; Zhang, M.; Li, H.; Shi, Y.; Dai, D. Silicon/2D-material photodetectors: From near-infrared to mid-infrared. *Light Sci. Appl.* **2021**, *10*, 1–21. [CrossRef] [PubMed]
77. Hu, F.; Dai, X.-Y.; Zhou, Z.-Q.; Kong, X.-Y.; Sun, S.-L.; Zhang, R.-J.; Wang, S.-Y.; Lu, M.; Sun, J. Black silicon Schottky photodetector in sub-bandgap near-infrared regime. *Opt. Express* **2019**, *27*, 3161–3168. [CrossRef] [PubMed]
78. Huang, S.; Wu, Q.; Jia, Z.; Jin, X.; Fu, X.; Huang, H.; Zhang, X.; Yao, J.; Xu, J. Black Silicon Photodetector with Excellent Comprehensive Properties by Rapid Thermal Annealing and Hydrogenated Surface Passivation. *Adv. Opt. Mater.* **2020**, *8*, 1901808. [CrossRef]
79. Huang, S.; Cao, J.; Song, G.; Cao, J.; Lu, Y.; Wu, Q.; Gao, W.; Xu, J. Broadband-Spectral-Responsivity of black silicon photodetector with high gain and sub-bandgap sensitivity by titanium hyperdoping. *Opt. Laser Technol.* **2024**, *171*, 110399. [CrossRef]